Structure and Morphology of Solution Blended Poly(vinylidene fluoride)/ Montmorillonite Nanocomposites

Valerio Causin, Massimo L. Carraro, Carla Marega, Roberta Saini, Sandro Campestrini, Antonio Marigo

Dipartimento di Scienze Chimiche, Università di Padova, via Marzolo 1, Padova 35131, Italy

Received 4 December 2007; accepted 6 March 2008
DOI 10.1002/app.28308
Published online 6 May 2008 in Wiley InterScience (www.interscience.wiley.com).

ABSTRACT: Nanocomposites based on poly(vinylidene fluoride) were prepared with montmorillonite by solution blending. The samples were characterized by small angle X-ray scattering, wide angle X-ray diffraction, Fourier transform infrared spectroscopy, and differential scanning calorimetry. Different crystallization conditions, that is, evaporation of the solvent and coprecipitation with two different antisolvents, H_2O or supercritical CO_2 ($scCO_2$), were tested and their influence on the resulting structure and morphology of the samples were studied. Coprecipitation with $scCO_2$ induced an ordinate crystalline framework and an intercalated morphology of clay, with a consequent large improvement in modulus.
 J Appl Polym Sci 109: 2354–2361, 2008

Key words: nanocomposites; poly(vinylidene fluoride); clay; SAXS; WAXS

INTRODUCTION

The large potential in property improvement associated with the addition of small fractions of nanofiller in a polymer matrix has aroused a relevant amount of research in the academic and industrial community.[1–3] Montmorillonite (MMT) is a smectite-type clay with a layered structure and is a very commonly employed nanofiller; each layer is 1 nm thick and has side dimensions ranging from 30 nm to several microns or more. The performance of polymer–clay nanocomposites depends on the breaking-up of clay particles in the polymer matrix. As the degree of interaction between polymer and filler varies, three systems are generally found: clay sheets may remain stacked in structures called tactoids, as in the original mineral without any improvement compared to usual microcomposites with a low filler loading; polymer chains may penetrate into interlayer spacing, producing an intercalated system where clay layers are more separated; finally, an exfoliated structure could appear, with the single clay sheets delaminated and dispersed in the matrix.

Among the possible matrices for polymer–clay nanocomposites, poly(vinylidene fluoride) (PVDF) is a very interesting one. PVDF is a partially fluorinated polymer with many interesting features and a broad range of applications.[4] Its outstanding mechanical properties characterize its use as an engineering material, while its good resistance to many chemical environments and to UV light makes it a suitable candidate in coating and membrane applications. Its piezoelectric behavior made PVDF an important material for many electronic applications. In general, PVDF has been a subject of active scientific research mainly for the interplay among the chemical structure, the thermomechanical history, and the crystal morphology. Three main crystal architectures (α, β, and γ) are obtained under ordinary crystallization conditions.[4–9] The most common polymorph, called α, has a monoclinic unit cell with a $TGT\overline{G}$ chain conformation.[5,8] The β phase is characterized by an orthorombic unit cell, with the chains in an all *trans* conformation.[4] The γ form has an orthorombic unit cell with $T_3GT_3\overline{G}$ chain conformation.[5,8,10] As an example, the piezoelectric and ferroelectric properties of PVDF are strictly related to the presence of one of these crystal phases (β phase).

Despite the attractive properties of this material, very few studies on PVDF-based nanocomposites have appeared in the literature. The first authors to report the preparation and properties of such materials were Priya and Jog.[11–13] Using a melt blending procedure, they obtained intercalated nanocomposites that crystallized in the β form. Among the other features of their samples there were an enhanced crystallization rate, a lower crystallinity degree, and increased storage modulus and glass transition

Correspondence to: V. Causin (valerio.causin@unipd.it).

temperature. Moussaif and Groeninckx[14] prepared PVDF-organoclay nanocomposites by melt blending in an extruder, using polymethylmethacrylate (PMMA) as an interfacial agent. PMMA was allowed to obtain nearly total exfoliation of clay in the polymer matrix, with large increases in storage modulus. Very remarkable results were reported by Shah et al.[15] They were able to simultaneously increase the stiffness and toughness of their PVDF-based nanocomposites. They also found that organoclay nucleated β phase, but concluded that it was the nanostructuring of the polymer induced by the nanoparticles, and not just β phase formation, to be responsible for the increase in properties of their materials. A mixed α-β polymorphism was observed in the PVDF-based nanocomposites prepared by Pramoda et al.[16,17] These authors reported very remarkable property improvements, such as an increased storage modulus and a decreased coefficient of thermal expansion.[16] Buckley et al. prepared nanocomposites with PVDF as a matrix and Lucentite, an organically modified silicate, as a filler.[18] They found that formation of the α or β polymorph were a function of filler content, with Lucentite favoring the formation of β phase. α phase disappeared when the added organoclay exceeded 0.5%. Time dependent WAXD studies showed that there was no conversion between α or β phases, while SAXS evidenced that the samples containing predominantly β form had less regular lamellar stacks, with fewer lamellae per stack.[18] Dillon et al. also studied the structure and morphology of PVDF-nanoclay nanocomposites.[19] They prepared their samples by solution casting and coprecipitation observing that the degree of clay dispersion varied as a function of the preparation method. Orientation phenomena and β phase nucleation were also reported by these authors.

Among the literature works about PVDF-based nanocomposites, just a few concerned samples prepared by solution blending,[18–20] while most authors used melt blending techniques. In this work nanocomposites were obtained from acetone solutions, and the effect of an antisolvent, either water or supercritical CO_2 ($scCO_2$), employed as a precipitating agent was investigated. In particular, $scCO_2$ was chosen because it is environmentally friendly, chemically inert, inexpensive, and nonflammable. From an industrial applicative point of view, using $scCO_2$ as an antisolvent has the advantage of avoiding liquid–liquid separation steps, as gaseous CO_2 spontaneously leaves the system after depressurization. If water is used in an acetone solution, it must be separated before the organic solvent can be recycled in the process. $scCO_2$ has been reported as a suitable solvent for *in situ* polymerized nanocomposites[21–23] or as a processing aid,[24,25] but its use as a precipitating agent is less frequent.[26–28]

Wide Angle X-ray Diffraction (WAXD), Small Angle X-ray Scattering (SAXS), Differential Scanning Calorimetry (DSC), and Fourier Transform Infrared Spectroscopy (FTIR) were used to characterize the samples, with the aim of studying the variations in the structure and morphology brought about by the preparation method and by the addition of clay.

EXPERIMENTAL

Samples and sample preparation

For the preparation of the composites, PVDF was purchased from Sigma-Aldrich Chemical (St. Louis, MO). This polymeric base was reported by the company to have $\bar{M}_w$ = 180,000 and $\bar{M}_n$ = 71,000, a melt flow rate of 24.3 g/10 min (230°C/3.8 kg, ASTM D 1238), and a melt viscosity of 6360 poise. Cloisite 15A (Southern Clay Products, Gonzales, TX), a montmorillonite ion-exchanged with octadecylammonium ions, was used as nanofiller. Acetone employed as a solvent was ACS reagent grade (≥99.5%) (Sigma-Aldrich, St. Louis, MO). All the above materials were used directly without any prior treatment.

PVDF and nanoclay, in the right proportions for obtaining each desired loading, were put in acetone. The magnetically stirred system was kept sealed at 100°C. When all the PVDF was dissolved and the clay was homogeneously dispersed, the system was allowed to cool down, still under agitation, to approximately 30°C. No precipitation of PVDF was observed during the cooling process. Films were prepared pouring the dispersion on Petri dishes and evaporating the solvent. When water was used as a precipitating agent, it was added to the acetone dispersion right after cooling down to 30°C. The precipitate thus formed was filtered and dried in an oven for 48 h. When $scCO_2$ was employed as an antisolvent, all the procedures were carried out in a closed steel vessel. The PVDF/clay/acetone mixture was heated at 100°C for 60 min, a time that was shown by preliminary tests to be suitable for total dissolution of PVDF. After that time, CO_2 (Air Liquide) was added by a syringe-type pump at 200 bar. These temperature and pressure conditions were chosen because they fall in the region of supercritical fluid for CO_2. PVDF has been reported to be soluble in $scCO_2$, but at temperatures and pressures far higher than those employed in this work.[29,30] After the treatments, the cell was depressurized to ambient pressure.

Wide angle X-ray diffraction

WAXD patterns were recorded in the diffraction angular range 1.5–30° 2θ by a Philips X'Pert PRO diffractometer, working in the reflection geometry and

equipped with a graphite monochromator on the diffracted beam (CuK_α radiation). The application of the least-squares fit procedure elaborated by Hindeleh and Johnson[31] gave the degree of crystallinity by weight which was then transformed in degree of crystallinity by volume[32] (ϕ_{WAXD}).

Small angle X-ray scattering

The SAXS patterns of the samples were recorded by an MBraun system, utilizing CuK_α radiation from a Philips PW 1830 X-ray generator. The data were collected by a position sensitive detector in the scattering angular range of 0.1–5.0° 2θ and they were successively corrected for blank scattering.

A constant continuous background scattering was then subtracted[33] and the obtained intensity values $\tilde{I}(s)$ were smoothed in the tail region, with the aid of the $s\tilde{I}(s)$ versus $1/s^2$ plot.[34]

Finally, the Vonk's desmearing procedure[35] was applied and the one-dimensional scattering function was obtained by the Lorentz correction $I_1(s) = 4\pi s^2 I(s)$, where $I_1(s)$ is the one-dimensional scattering function and $I(s)$ the desmeared intensity function, being $s = (2/\lambda)\sin\theta$.

SAXS data analysis

The evaluation of the SAXS patterns according to some theoretical distribution models[36] was carried out referring to the Hosemann model,[37] that assumes the presence of lamellar stacks having an infinite side dimension. This assumption takes into account a monodimensional electron density change along the normal direction to the lamellae.

The intensity profile was evaluated as:

$$I(s) = I^I(s) + I^{II}(s)$$

where

$$I^I(s) = \frac{(\rho_C - \rho_A)^2}{4\pi^2 s^2 D} \times \frac{|1 - F_C|^2\left(1 - |F_A|^2\right) + |1 - F_A|^2\left(1 - |F_C|^2\right)}{|1 - F_C F_A|^2}$$

$$I^{II}(S) \stackrel{I}{=} \frac{(\rho_C - \rho_A)^2}{2\pi^2 s^2 DN} \times \mathrm{Re}\left\{\frac{F_A(1 - F_C)^2\left(1 - (F_C F_A)^N\right)}{(1 - F_C F_A)^2}\right\}$$

In these equations, F_C and F_A represent the Fourier transforms of the distribution functions of the crystalline and of the amorphous regions, respectively, ρ_C and ρ_A are the electron densities of the crystalline and amorphous regions, respectively, N is the average number of polymeric lamellae in the stacks, and D the average long period. A fitting procedure of the calculated one-dimensional scattering functions with the experimental ones allows to optimize the values of the crystalline (C) and amorphous (A) region thicknesses. Crystallinity (ϕ_{SAXS}) was evaluated as the ratio between the thickness of the crystalline regions over the long period $D = A + C$.

Fourier transform infrared spectroscopy

Infrared (IR) absorption spectra were acquired in attenuated total reflection (ATR) on a Nicolet 5700 FTIR spectrometer (Thermo Nicolet) equipped with a Smart Performance accessory (Thermo Nicolet) with a ZnSe crystal. The spectral region spanned from 4000 to 500 cm^{-1}, with a resolution of 4 cm^{-1}, and 256 acquisitions were gathered.

Differential scanning calorimetry

Differential Scanning Calorimetry measurements were carried out with a model 2920 calorimeter (TA Instruments) operating under N_2 atmosphere. The samples, weighing about 5 mg, were closed in aluminum pans. After erasure of thermal history by a 5 min isotherm at 190°C, the samples were cooled down to room temperature at 10°C/min and heated again to 190°C at the same rate. Indium of high purity was used for calibrating the DSC temperature and enthalpy scales.

Flexural modulus

The flexural modulus of the samples (dimension 25 mm × 5 mm × 2 mm) were measured using an Instron Model 3345 mechanical tester at room temperature. The crosshead speed was 1 mm min^{-1}. At least five measurements were performed for each composite.

RESULTS AND DISCUSSION

FTIR spectroscopy was used to study the polymorphism of PVDF in the samples. The signals characteristic of the α phase of PVDF are at 530, 614, 763, 795, and 870 cm^{-1}.[13,15,16,18,38,39] The β phase can be detected by the CF bending absorption at 510 cm^{-1} and by the CH_2 rocking signal at 840 cm^{-1}.[13,15,16,38,39] γ phase gives a distinguished peak at 1230 cm^{-1}.[18,38] Along with the principal α phase signal at 870 cm^{-1}, it can be seen in Figure 1 that also β and γ form characteristic peaks coexist in all the FTIR spectra of the samples pertaining to the series prepared by solution blending in acetone.

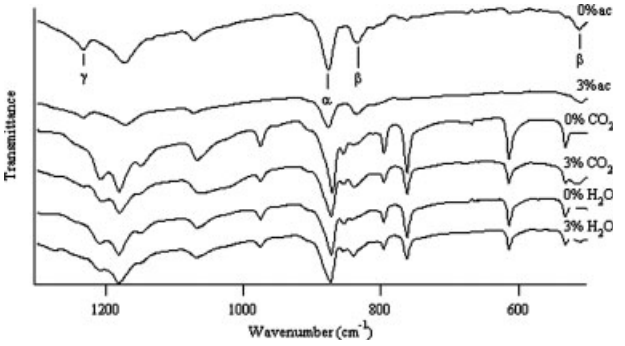

Figure 1 FTIR spectra of the samples. The characteristic signals of each polymorph are shown.

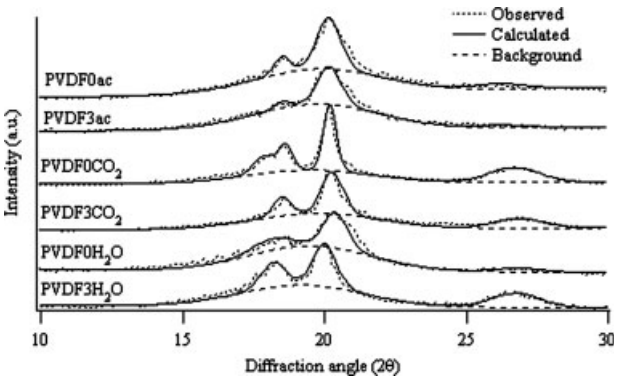

Figure 2 WAXD patterns of the samples. The functions used for fitting of experimental data are also shown.

WAXD experiments were performed to confirm these findings (Fig. 2). The α phase of PVDF exhibits four main reflections at about 17.8, 18.5, 20.1, and 26.7° 2θ, corresponding to the (100), (020), (110), and (021) planes, respectively.[18,19,40] The β phase, on the other hand, has a main characteristic peak at about 20.5° 2θ, due to the (110) and (200) reflections.[4,12,15,16,18,19,38] The γ phase shows a diffraction profile very similar to the sum of the α and β polymorphs, so it is hardly possible to distinguish this form by WAXD.[4,18] Pure PVDF and the 3% composite that underwent the dissolution process in acetone with subsequent crystallization by evaporation displayed two main, broad peaks at 18.5 and 20.3° 2θ, respectively. The first reflection was ascribable to the $(020)_\alpha$ planes of α phase, while the second one was probably due to the overlap of the $(110)_\alpha$ signal of the α form and the $(110)_\beta/(200)_\beta$ peak of the β polymorph. It is interesting to note that only the most intense signals of the α phase were visible in both IR and WAXD patterns. The remaining α form peaks were very weak and barely detectable. This is possibly a consequence of the relatively poor crystalline order of these samples. α, β, and γ phases of PVDF thus form simultaneously when the polymer is allowed to slowly crystallize as the solvent evaporates. The formation of β and γ phases by crystallization from solution has been already reported in the literature.[4,5,10] The decrease in intensity of the $(020)_\alpha$ signal of the α form in the WAXD spectra of sample PVDF3ac is coherent with the nucleating effect of clay that favors the β polymorph.[11–13,15–19]

The effects of an antisolvent on the structure and morphology were also tested. Figures 1 and 2 show the FTIR and WAXD spectra of the coprecipitated samples. The samples of pure PVDF prepared by precipitation with water or $scCO_2$ as an antisolvent displayed just α phase. The WAXD pattern of sample PVDF0CO_2 shows in fact a typical α form profile, with all the characteristic peaks clearly visible, and in the FTIR spectrum the signals at 510 and 840 cm^{-1} were absent. No 510 and 840 cm^{-1} peaks were observed in sample PVDF0H_2O, as well, but in the WAXD diffractogram the α peaks were less sharp and intense than in PVDF0CO_2, probably as a consequence of the small dimension of crystallites. Table I reports the degrees of crystallinity measured by deconvolution of WAXD spectra.[31] If pure PVDF samples are compared, it can be seen that coprecipitation with $scCO_2$ brought about a remarkable increase in the degree of crystallinity. On the contrary, when water was used as an antisolvent, the crystallinity was lower. These opposite behaviors could be ascribed to the different effects on the polarity of the medium brought about by the two antisolvents. Water increases the polarity, $scCO_2$ makes the system less polar, possibly favoring an ordinate

TABLE I
Formulation and Morphological and Structural Features of the Studied Samples

Sample	% Clay	Antisolvent	ϕ_{WAXS} (%)	ϕ_{SAXS} (%)	*C* (Å)	*A* (Å)	*D* (Å)
PVDF0ac	0	–	38	46	56	65	121
PVDF3ac	3	–	27	38	57	93	150
PVDF0H_2O	0	H_2O	32	44	78	100	178
PVDF3H_2O	3	H_2O	47	52	90	83	173
PVDF0CO_2	0	$scCO_2$	59	61	128	83	211
PVDF3CO_2	3	$scCO_2$	48	50	66	65	131

The degree of crystallinity determined by WAXD and SAXS (ϕ_{WAXD} and ϕ_{SAXS}, respectively), the thickness of the crystalline (*C*) and amorphous layer (*A*) and the long period (*D*) are shown.

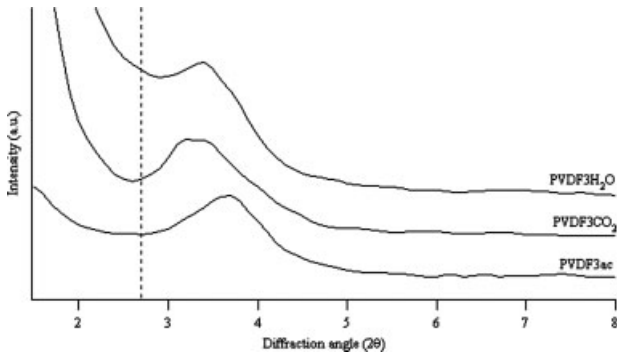

Figure 3 WAXD patterns of composite samples in the clay tactoids' periodicity region. The dashed line marks the position of the basal peak in pristine montmorillonite.

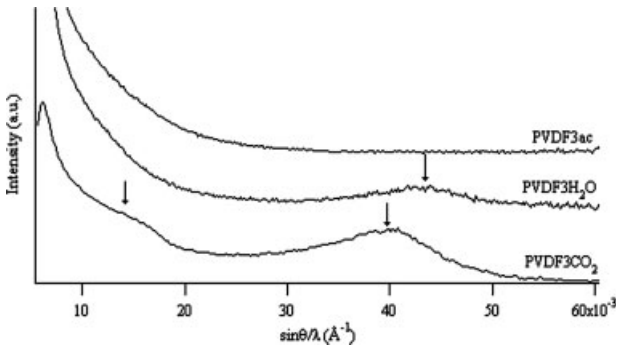

Figure 4 SAXS patterns of composite samples in the clay tactoids' periodicity region. The arrows point to the signals due to the stacking of clay layers.

crystallization of PVDF. This can be confirmed by examining the composite samples, among which PVDF3CO_2 is the most crystalline. For what concerns the series prepared in acetone and the sample coprecipitated by scCO_2, clay exerts a disruptive effect on the regular ordering of polymer chains. The crystallinity of the composites is in fact lower than that of the correspondent matrix. This effect has already been observed in PVDF[11–13,18,19,39] and in a number of polymer–clay nanocomposite systems.[41,42] A competition between enhanced nucleation and reduction of chain mobility due to clay has been advocated as the reason for this decrease in crystallinity.[18] This may be the reason why we observed a different behavior in the composite prepared by coprecipitation with water. PVDF3H_2O showed a higher crystallinity than the corresponding matrix PVDF0H_2O, differently from what was reported by Dillon et al., who found a decrease in crystallinity with this technique also.[19] These authors ascribed this decrease to the nanoconfinement of the polymer in intercalated nanocomposites. In our samples coprecipitated with water we did not obtain intercalation (Fig. 3), so probably the increased polarity due to water enhanced the nucleation activity of clay that, in this case of a phase separated composite, was predominant on the reduction of chain mobility.

The low angle portion of the WAXD patterns of the nanocomposites are shown in Figure 3. The basal signal of clay is located at wider angles than pristine montmorillonite, i.e., clay layers collapsed probably as a consequence of an altered conformation of the organic modifier or of the extraction of the organic modifier by a concurrent action of solvent and polymer. Solvent alone was not sufficient to extract the modifier, as was confirmed by treatment, in the same conditions of preparation of the nanocomposites, of clay with acetone, which did not bring about any shift in the basal peak position. SAXS was used to check if intercalation had enlarged the clay interlayer space to values exceeding those observable by WAXD. Just one peak, at periodicities of about 23 Å, consistent with that observed by WAXD and relative to collapsed clay, was recorded for sample PVDF3H_2O. Sample PVDF3CO_2 showed two maxima (Fig. 4). Intercalation was therefore attained only for the composite prepared by coprecipitation with scCO_2, whereas in the other cases collapse of the layers was observed. The featurless SAXS signal of sample PVDF3ac is consistent with a very disordered and heterogenous morphology of tactoids, composed by very few layers.[19,42,43] In the composite coprecipitated with scCO_2, the basal peak split into two signals: one is due to intercalated clay, in which the interlayer distance is increased up to about 70 Å, and the other is due to collapsed clay layers, with a periodicity of 25 Å. Intercalated and exfoliated structures are known to be metastable.[19] When crystallization by simple evaporation of the solvent or precipitation by water were used, the kinetics of crystallization were probably not fast enough and the clay layers were allowed to return to their pristine stacked morphology. The crystallization conditions brought about by scCO_2 were on the other hand suitable to freeze the metastable structure attained

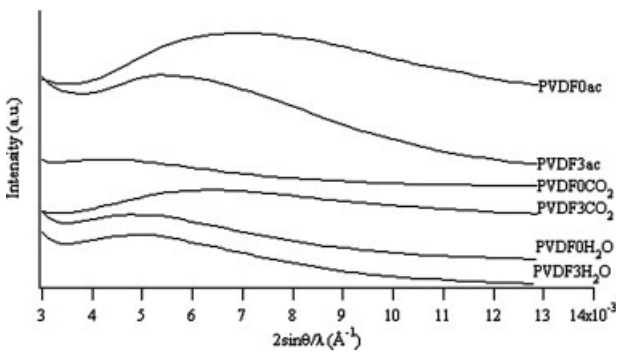

Figure 5 SAXS patterns in the polymer lamellar periodicity region of samples crystallized by solution casting and by precipitation with water or scCO_2 as antisolvents.

TABLE II
Flexural Modulus of the Samples

% Clay	Antisolvent	Modulus (MPa)
0	–	734
3	–	1017 (38%)
3	H_2O	904 (23%)
3	$scCO_2$	1083 (48%)

Values in parentheses represent percentage increase as compared to blank PVDF.

by the system while in solution, so intercalated clay was obtained.

SAXS was also used to investigate the morphology of polymeric lamellar stacks (Fig. 5). The results are summarized in Table I. In the series prepared by solution casting in acetone, the disruptive effect of clay can be very clearly visualized. Especially at low-clay contents, when aggregation of tactoids is less severe and the aspect ratio of the filler is higher, a very large increase in the thickness of the amorphous layer is seen relative to the pristine matrix, while the thickness of the crystalline layer remains nearly constant. These changes in the lamellar morphology are mirrored by the degree of crystallinity measured by SAXS, which displays the same trend as the crystallinity degree evaluated by WAXD. It can be seen that the crystallinities assessed by SAXS have larger values relative to those estimated by WAXD. This divergence can be explained considering the difference between the two techniques. SAXS is only sensitive to the crystalline regions organized in lamellar stacks, whereas WAXD allows the detection of all the regions contributing to the semicrystalline framework, including the amorphous phase located between the lamellar stacks. Therefore, WAXD crystallinity is lower because the contribution of crystalline domains is ''diluted'' by the interstack amorphous.[41–46]

If the pristine matrices are compared to study the effect of sample preparation, WAXD results were confirmed. Coprecipitation with $scCO_2$ was the most suitable method to promote a regular ordering of the polymer, also at a lamellar level. The thickness of the crystalline layer in sample PVDF0CO_2 was more than double that of PVDF crystallized from acetone. The largest long period and the highest crystallinity were also obtained by using $scCO_2$ as an antisolvent. It is interesting to note that in the case of pristine PVDF and of its composite with 3% clay prepared by precipitation with $scCO_2$, φ_{SAXS} and φ_{WAXD} coincide. This means that a particularly ordered crystalline framework was obtained under this condition, with all the crystalline domains ordered into lamellar stacks. The use of water as an antisolvent promoted an increase in long period with respect to PVDF crystallized from acetone, but the proportion of the amorphous and crystalline phases increased pretty much by the same amount, so the degree of crystallinity did not differ much from that of the other sample.

When the samples filled with 3% clay were taken into account, the trend of morphological data resembled that found by WAXD. By this technique also the degrees of crystallinity of precipitated samples were larger than that of the solution cast one. SAXS evidenced that clay diminished the degree of crystallinity of the solution cast and of the $scCO_2$ coprecipitated samples with respect to the pristine matrix, while an increase in crystallinity at a lamellar level as well was promoted by water as an antisolvent. Lamellar thicknesses confirmed these conclusions. The reason for these opposite trends in coprecipitated samples can be in the different effect on the polarity of the system brought about by water and $scCO_2$. Water and $scCO_2$ produced opposite effects also on the flexural modulus of the materials (Table II). All clay containing samples showed much superior moduli with respect to pristine PVDF.[11,12,16,47] Comparing the 3% filled samples, it can be seen that the lowest modulus is that of PVDF3H_2O and the highest that of PVDF3CO_2. The nanocomposite prepared by coprecipitation with $scCO_2$, with its ordered semicrystalline framework and an intercalated clay structure allowed for the best improvement in physical mechanical properties. The effect of the intercalation of clay on the modulus

TABLE III
Melting Temperatures Obtained in the First and Second Heating Run (T_{m1} and T_{m2}, respectively) and Crystallization Temperature (T_c) Obtained in the Cooling Run of DSC Experiments

Sample	% Clay	Antisolvent	T_{m1} (°C)	T_c (°C)	T_{m2} (°C)
PVDF0ac	0	–	164.6	136.4	164.6, 167.8 (s)
PVDF3ac	3	–	161.6 (s), 169.3	148	166.2 (s), 173.2
PVDF0H_2O	0	H_2O	157.8 (s), 167.8	137.7	165.8
PVDF3H_2O	3	H_2O	158.4 (s), 167.6, 175.3 (s)	143.8	156.1 (s), 173.9
PVDF0CO_2	0	$scCO_2$	152.4, 164.7	140.1	164.3, 172.1
PVDF3CO_2	3	$scCO_2$	155 (s), 166.8, 174.0	148.8	174.5

can be seen comparing samples PVDF3H_2O and PVDF3CO_2. These two samples have similar degrees of crystallinity, but they differ much in modulus. The property increase of PVDF3CO_2 is thus principally ascribable to the intercalation of clay.

The thermal behavior of the samples was studied by DSC. Multiple melting peaks were observed in all the samples, except in the case of neat PVDF crystallized from acetone and coprecipitated with water. Multiple melting behavior is a common feature of PVDF-based nanocomposites and has been mainly ascribed to different crystal populations.[18,19] In Table III, it can be noted that both melting and crystallization temperatures increased as a consequence of the addition of clay. For what concerns the melting temperature, the increase is due to clay favoring formation of β phase. This polymorph has a higher melting point than the α phase, so its increase shifts the melting peak of the composite samples towards higher values.[11–13,16,18,19] The increase in crystallization temperature is on the other hand consistent with the nucleation effect of clay, as confirmed by reports in the literature.[11,16,19,48]

CONCLUSIONS

In this work, the structure and morphology of PVDF/montmorillonite nanocomposites were studied. The polymorphic behavior of PVDF was confirmed to be dependent on the nucleating effect of clay, which favored formation of β phase. The use of different antisolvents, scCO_2 or H_2O, for the precipitation of the composites brought about different structures and morphologies. Water induced a lower crystallinity in neat PVDF, if compared to the polymer crystallized by solvent evaporation, while coprecipitation with scCO_2 increased the crystallinity of the pristine matrix. Clay, on the other hand, exerted a disruptive role on the regular ordering of polymer chains in the case of scCO_2, whereas water enhanced the crystallization. The reason of this opposite behavior should be sought in the different effects on the polarity of the medium, which is increased by water and decreased by scCO_2, and on the different degree of dispersion of MMT. Another factor that has a role in shaping the morphology of the samples is the crystallization kinetics. Just in the case of scCO_2 it was possible to intercalate clay, because crystallization was fast enough to freeze the metastable structure attained by the system while in solution. scCO_2 moreover promoted more regular lamellar stacks. Because of its ordinate crystalline framework and its intercalated morphology, the nanocomposite prepared by coprecipitation with scCO_2 also showed the largest improvement in modulus. The use of scCO_2 as an antisolvent is therefore a suitable method to prepare intercalated PVDF-based nanocomposites with the solvent blending method.

References

1. LeBaron, P. C.; Wang, Z.; Pinnavaia, T. J Appl Clay Sci 1999, 15, 11.
2. Ray, S. S.; Okamoto, M. Prog Polym Sci 2003, 28, 1539.
3. Morgan, A. B. Mater Matters 2007, 2, 20.
4. Lovinger, A. J. In Developments in Semicrystalline Polymers; Bassett, D. C., Ed.; Applied Science Publisher: Oxford, 1982, p 195.
5. Hasegawa, R.; Kobayashi, M.; Takodoro, H. Polym J 1972, 3, 591.
6. Lovinger, A. J.; Davis, D. D.; Cais, R. E.; Kometani, J. M. Polymer 1987, 28, 617.
7. Marega, C.; Marigo, A. Eur Polym Mater 2003, 39, 1713.
8. Nandi, A. K.; Mandelkern, L. J Polym Sci Part B: Polym Phys 1991, 29, 1287.
9. Prest, W. M.; Luca, D. J. J Appl Phys 1975, 46, 4136.
10. Tazaki, M.; Wada, R.; Okabe, M.; Homma, T. J Appl Polym Sci 1997, 65, 1517.
11. Priya, L.; Jog, J. P. J Polym Sci Part B: Polym Phys 2002, 40, 1682.
12. Priya, L.; Jog, J. P. J Polym Sci Part B: Polym Phys 2003, 41, 31.
13. Priya, L.; Jog, J. P. J Appl Polym Sci 2003, 89, 2036
14. Moussaif, N.; Groeninckx, G. Polymer 2003, 44, 7899.
15. Shah, D.; Maiti, P.; Gunn, E.; Schmidt, D. F.; Jiang, D. D.; Batt, C. A.; Giannelis, E. P. Adv Mater 2004, 16, 1173.
16. Pramoda, K. P.; Mohamed, A.; Phang, I. Y.; Liu, T. Polym Int 2005, 54, 226.
17. Pramoda, K. P.; Tay, S. S.; Liu, T.; Sprenger, P. Polym Eng Sci 2006, 46, 1684.
18. Buckley, J.; Cebe, P.; Cherdack, D.; Crawford, J.; Ince, B. S.; Jenkins, M.; Pan, J.; Reveley, M.; Washington, N.; Wolchover, N. Polymer 2006, 47, 2411.
19. Dillon, D. R.; Tenneti, K. K.; Li, C. Y.; Ko, F. K.; Sics, I.; Hsiao, B. S. Polymer 2006, 47, 1678.
20. Liu, H. J.; Hwang, J. J.; Chen-Yang, Y. W. J Polym Sci Part A: Polym Chem 2002, 40, 3873.
21. Zerda, A. S.; Caskey, T. C.; Lesser, A. J. Macromolecules 2003, 36, 1603.
22. Yan, C.; Ma, L.; Yang, J. C. J Appl Polym Sci 2005, 98, 22.
23. Yue, B.; Wang, Y.; Huang, C.; Pfeffer, R.; Iqbal, Z. J Nanosci Nanotechnol 2007, 7, 994.
24. Zhao, Q.; Samulski, E. T. Macromolecules 2003, 36, 6967.
25. Yang, K.; Ozisik, R. Polymer 2006, 47, 2849.
26. Zhang, J. L.; Liu, Z. M.; Han, B. X.; Liu, D. X.; Chen, J.; He, J.; Jiang, T. Chem Eur J 2004, 10, 3531.
27. Li, Z. H.; Zhang, J. L.; Du, J. M.; Mu, T. C.; Liu, Z. M.; Chen, J.; Han, B. X. J Appl Polym Sci 2004, 94, 1643.
28. Zhang, J. L.; Liu, Z. M.; Han, B. X.; Li, J. C.; Li, Z. H.; Yang, G. Y. J Nanosci Nanotechnol 2005, 5, 945.
29. Lora, M.; Lim, J. S.; McHugh, M. A. J Phys Chem B 1999, 103, 2818.
30. Di Noia, T. P.; Conway, S. E.; Lim, J. S.; McHugh, M. A. J Polym Sci Part B: Polym Phys 2000, 38, 2832.
31. Hindeleh, A. M.; Johnson, D. J. J Phys D Appl Phys 1971, 4, 259.
32. Glatter, O.; Kratky, O., Ed. Small Angle X-ray Scattering; Academic press: London, 1982; p 433.
33. Vonk, C. G.; Pijpers, A. P. J Polym Sci Part B: Polym Phys 1985, 23, 2517.
34. Vonk, C. G. J Appl Crystallogr 1973, 6, 81.
35. Vonk, C. G. J Appl Crystallogr 1971, 4, 340.
36. Marega, C.; Marigo, A.; Cingano, G.; Zannetti, R.; Paganetto, G. Polymer 1996, 37, 5549.

37. Hosemann, R.; Bagchi, S. N. Direct Analysis of Diffraction by Matter; North Holland: Amsterdam, 1962.
38. Yee, W. A.; Kotaki, M.; Liu, Y.; Lu, X. Polymer 2007, 48, 512.
39. Shieh, Y.; Hsiao, T.; Chang, S. Polymer 2006, 47, 5929.
40. Bachmann, M.; Lando, J. Macromolecules 1981, 14, 40.
41. Causin, V.; Marega, C.; Marigo, A.; Ferrara, G.; Idiyatullina, G.; Fantinel, F. Polymer 2006, 47, 4773.
42. Causin, V.; Marega, C.; Marigo, A.; Ferrara, G.; Ferraro, A.; Selleri, R. J. Nanosci Nanotechnol 2008, 8, 1823.
43. Causin, V.; Marega, C.; Marigo, A.; Ferrara, G. Polymer 2005, 46, 9533.
44. Benetti, E.; Causin, V.; Marega, C.; Marigo, A.; Ferrara, G.; Ferraro, A.; Consalvi, M.; Fantinel, F. Polymer 2005, 46, 8275.
45. Causin, V.; Marega, C.; Marigo, A.; Ferrara, G.; Ferraro, A. Eur Polym Mater 2006, 42, 3153.
46. Marega, C.; Causin, V.; Marigo, A. Macromol Res 2006, 14, 588.
47. Kim, Y.; White, J. L. J Appl Polym Sci 2004, 92, 1061.
48. Causin, V.; Marega, C.; Saini, R.; Marigo, A.; Ferrara, G. J Therm Anal Calorimetry 2007, 90, 849.